Key Points:
- The stratospheric injection of SO_2 would result in localized stratospheric warming
- This warming would modify the thermal wind balance, strengthening the stratospheric polar vortexes
- This results in less poleward transport of the aerosols, requiring more SO_2 to achieve the desired cooling

Reduced Poleward Transport Due to Stratospheric Heating Under Stratospheric Aerosols Geoengineering

Daniele Visioni[1] [ID], **Douglas G. MacMartin**[1] [ID], **Ben Kravitz**[2,3] [ID], **Walker Lee**[1] [ID], **Isla R. Simpson**[4] [ID], and **Jadwiga H. Richter**[4] [ID]

[1]Sibley School for Mechanical and Aerospace Engineering, Cornell University, Ithaca, NY, USA, [2]Department of Earth and Atmospheric Science, Indiana University, Bloomington, IN, USA, [3]Atmospheric Sciences and Global Change Division, Pacific Northwest National Laboratory, Richland, WA, USA, [4]Climate and Global Dynamics Laboratory, National Center for Atmospheric Research, Boulder, CO, USA

Abstract By injecting SO_2 into the stratosphere at four latitudes (30°, 15°N/S), it might be possible not only to reduce global mean surface temperature but also to minimize changes in the equator-to-pole and inter-hemispheric gradients of temperature, further reducing some of the impacts arising from climate change relative to equatorial injection. This can happen only if the aerosols are transported to higher latitudes by the stratospheric circulation, ensuring that a greater part of the solar radiation is reflected back to space at higher latitudes, compensating for the reduced sunlight. However, the stratospheric heating produced by these aerosols modifies the circulation and strengthens the stratospheric polar vortex which acts as a barrier to the transport of air toward the poles. We show how the heating results in a feedback where increasing injection rates lead to stronger high-latitudinal transport barriers. This implies a potential limitation in the high-latitude aerosol burden and subsequent cooling.

Plain Language Summary If we were to inject aerosols at high altitudes in order to reflect some incoming solar radiation and cool the planet, it would result in a localized warming at those altitudes. This would affect the circulation of air masses, and we show here that it would reduce the intensity of the transport of air from the mid-latitudes to the poles. If this transport is reduced, less aerosol can reach the high latitudes, making it harder to achieve a distribution of aerosols that would offset global warming evenly.

1. Introduction

Stratospheric aerosol geoengineering (SAG) involves deliberately injecting aerosols or their precursors into the stratosphere in an attempt to cool the planet, mimicking the cooling seen after large volcanic eruptions (Budyko, 1977; Crutzen, 2006). Climate model simulations generally agree that injecting SO_2 has the potential to reduce global surface temperatures relative to the warming induced by greenhouse gases (GHGs); the imperfect compensation between the GHG and SO_2 forcing (Govindasamy et al., 2003; Jiang et al., 2019) would, however, result in differences in aspects of the surface climate such as the hydrological cycle (Niemeier et al., 2013; Simpson et al., 2019; Tilmes et al., 2013) compared to a non-geoengineered climate with no GHG warming, but these differences would still be much lower than those resulting from continued GHG-induced warming (Irvine & Keith, 2020). Large uncertainties are still present in many areas related to the possible interactions with different aspects of the climate (Kravitz & MacMartin, 2020).

One of the most important perturbations resulting from the injection of SO_2 is the stratospheric heating resulting from the increase in aerosol heating rates. Modifications in the stratospheric transport, observed in the past in the case of large volcanic eruptions (Pitari et al., 2016; Robock, 2000), are consistently found in SAG simulations (Kleinschmitt et al., 2018; Niemeier & Schmidt, 2017; Richter et al., 2017; Visioni et al., 2017). Aquila et al. (2014) first pointed out the potential of equatorial SAG to interact with stratospheric dynamics by modifying the quasi-biennial oscillation (QBO), resulting, already for an injection load of 5 Tg-SO_2, in a permanent locking of the QBO in a westerly phase. That phase of the QBO results in stronger aerosol confinement in the tropical pipe due to decreased meridional transport and increased residual vertical velocities, which result in greater sulfate aerosol growth (Kravitz et al., 2019; Niemeier & Schmidt, 2017;

Visioni et al., 2018). Larger sulfate aerosols are less effective at backscattering insolation and have reduced particle lifetimes (Pierce et al., 2010), reducing the SO_4 burden and resulting global aerosol optical depth (AOD) that results from a given SO_2 injection rate. Some studies (Benduhn et al., 2016; Pierce et al., 2010) have proposed that the injection of H_2SO_4 droplets instead of SO_2 might produce an aerosol size distribution with smaller particles, capable of reflecting more solar radiation per unit mass (Dykema et al., 2016), thus potentially reducing some of the side effects related to the heating produced by the aerosols (Vattioni et al., 2019); other aerosol choices might result in less, or even no, stratospheric heating (Keith et al., 2016).

Injecting outside of the equator has been shown to better manage desired temperature targets and to reduce some of the side effects of equatorial injections mentioned above (Dai et al., 2018; Kravitz et al., 2019; Richter et al., 2017; Tilmes, Richter, Mills, et al., 2018; Tilmes et al., 2017). By injecting at 15°N, 30°N, 15°S, and 30°S in the Geoengineering Large Ensemble simulations performed with the Community Earth System Model (CESM1(WACCM)), it was possible to produce a stratospheric aerosol layer capable of reducing global mean temperatures over the course of the 21st century as well as restoring the inter-hemispheric and equator-to-pole temperature gradients affected by the increasing GHG concentration. Managing these additional temperature goals, however, requires part of the aerosol distribution to reach the very high latitudes.

A strong stratospheric polar vortex inhibits aerosol transport to high latitudes and results in greater confinement of polar stratospheric air. As such, one measure of the transport of stratospheric air from the mid-latitudes to the poles is the strength of the stratospheric polar vortex (Waugh et al., 2017). In the two hemispheres, westerly zonal winds at and above 50 hPa have a peak in strength at approximately 60° latitude in winter. Projecting future changes in the polar vortex is difficult, as they will be influenced by stratospheric cooling from GHGs, as well as projected reductions in ozone-depleting substances (ODS Dhomse et al., 2018) and changes in the wave driving from the troposphere (Manzini et al., 2014). Models tend to disagree on the sign and magnitude of net vortex changes (Butchart et al., 2010; Manzini et al., 2014; Simpson et al., 2018; Wu et al., 2019).

In this work, we show that, for SAG simulations, the perturbation produced by the stratospheric heating even in non-equatorial SAG results in a strengthening of the polar vortex in both hemispheres, resulting in a reduced transport of aerosols from the mid-latitudes to the poles and, ultimately, in decreased high-latitude AOD per Tg-SO_2 injected. This suggests that additional injection poleward of the polar vortex may be needed to avoid an undercooling of the poles.

2. Methods

The simulations analyzed in this paper have been performed with the Community Earth System Model (CESM1(WACCM)), with a resolution of 0.95° × 1.25°, 70 vertical levels and fully interactive stratospheric chemistry (Mills et al., 2017).

The analyses presented here are based on two ensembles of SAG simulations. The first, the Geoengineering Large Ensemble (GLENS; Tilmes, Richter, Kravitz, et al., 2018), involves independently modifying the annual SO_2 injection (5 km above the mean tropopause) rate at 30°N, 15°N, 15°S, and 30°S to maintain (against a background of RCP8.5) three temperature metrics at their 2010–2030 average levels: global mean temperature, the inter-hemispheric temperature gradient, and the equator-to-pole temperature gradient. The second ensemble, labeled GEQ, involves modifying the annual SO_2 injection rate at the equator to maintain global mean temperature at its 2010–2030 average level, also against a background of RCP8.5 (Kravitz et al., 2019). These objectives were met using a feedback algorithm (Kravitz et al., 2016, 2017) to independently adjust the SO_2 injection rates at each location based on past departures from the intended temperature targets. An ensemble of 21 baseline simulations were conducted with RCP8.5 from 2010 to 2030; four of these were extended until at least 2098. The 21-member GLENS ensemble branched from these simulations in 2020 and were run until 2100. For GEQ, three simulations were conducted.

3. Results

In GLENS, annual mean global average AOD and tropical stratosphere sulfate aerosol effective radius both scale proportionally with the annual SO_2 injection rate (Tilmes, Richter, Kravitz, et al., 2018). This result
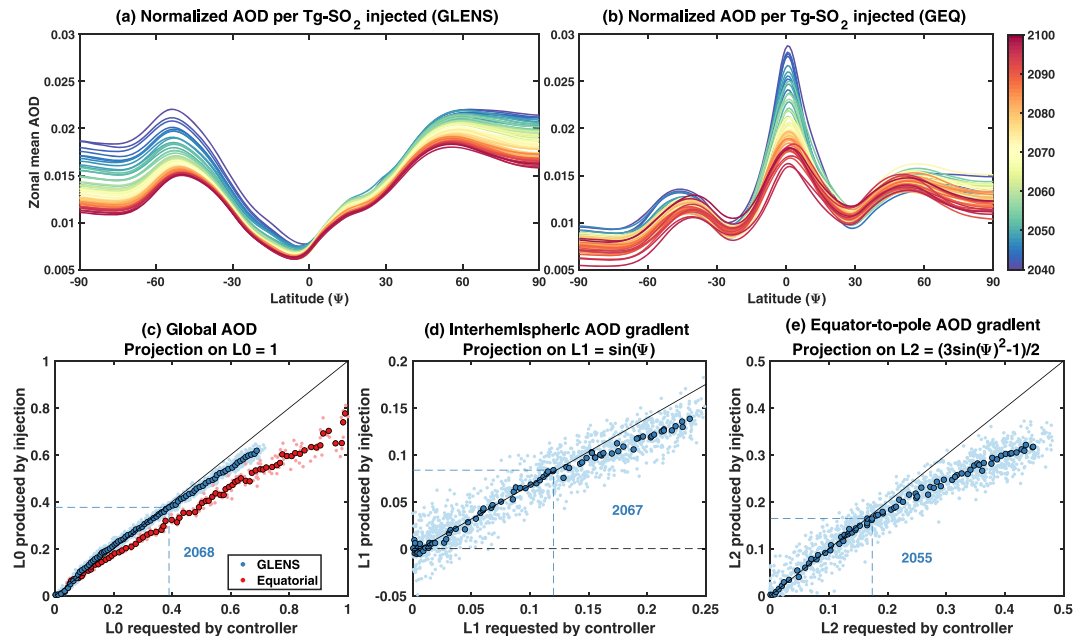
Figure 1. (top panels) Zonal mean AOD (a) for GLENS, and (b) for GEQ normalized to the amount of SO_2 injected in the year before, and color coded by year. (bottom panels) Projections of AOD onto the first three Legendre polynomials; the ability to choose injection rates at different latitudes to independently alter these patterns of AOD is used by the controller to manage global mean temperature (using global mean AOD, L0, shown in panel c), inter-hemispheric temperature gradient (using AOD projected over a linearly increasing function from south to north, L1, shown in panel d), and equator-to-pole temperature gradient (using AOD projected over a quadratic function maximized at the poles and minimized at the equator, L2, shown in panel e). The values requested by the controller in each year are plotted against the actual L0, L1, and L2 values of the AOD. A linear fit for small values of the three quantities is provided, with the threshold where the linear relationship stops being true highlighted. In Figure S1 in the supporting information, we show the differences in the zonal mean AOD in the last 20 years of simulation between the expected and actual distribution.

differs from earlier results given for equatorial injections (Niemeier & Timmreck, 2015) and has been concluded to be a direct result of the injection strategy (Kravitz et al., 2019; Tilmes, Richter, Kravitz, et al., 2018). In Figure 1, we show that this conclusion mostly holds true when looking at globally averaged AOD because the globally averaged value heavily weights tropical latitudes, where the linear scaling holds. In the extra-tropics, the relationship between AOD and injection rate is, on the other hand, non-constant. To highlight the difference between the two injection strategies, Figure 1b shows the same values for GEQ, where there is a clear sublinear relationship between SO_2 injection rate and AOD in the tropical pipe, which we attribute to the microphysical effects discussed previously.

The effects of this "diminishing return" in the efficiency (by which here we mean the ratio of produced AOD to injected aerosol precursors) of the injection at high latitudes is shown in the bottom panels in Figure 1, depicting zonally averaged AOD projected onto the first three Legendre polynomials (denoted ℓ_0, ℓ_1, and ℓ_2 for the projection onto L0 = 1, L1 = sin(ψ), and L2 = $3(\sin^2(\psi)-1)/2$, where ψ is the latitude). As shown in previous works (Kravitz et al., 2016; MacMartin et al., 2013), the solar constant can be reduced across these three idealized patterns to not only reduce global mean temperature (termed T0) but also maintain the inter-hemispheric temperature gradient (T1) and equator-to-pole temperature gradient (T2). By means of injecting at different latitudes, it has been shown that it is possible to achieve similar spatial patterns for AOD, capable of reflecting sunlight across the three patterns and thus achieving the three temperature goals (MacMartin et al., 2017). Because AOD must be positive at all latitudes and injection rates must be positive, the values of ℓ_1 and ℓ_2 are constrained (with $|\ell_1| + \ell_2 \leq \ell_0$, where the values are those requested by the controller—not those actually produced). In the GLENS simulations, the value of ℓ_2 was always constrained to its maximum value, not quite sufficient to manage T2.

The correlation between injected SO_2 at the four locations and resulting AOD in MacMartin et al. (2017) assumes that the relationship would remain linear for different injection loads. From the bottom panels in
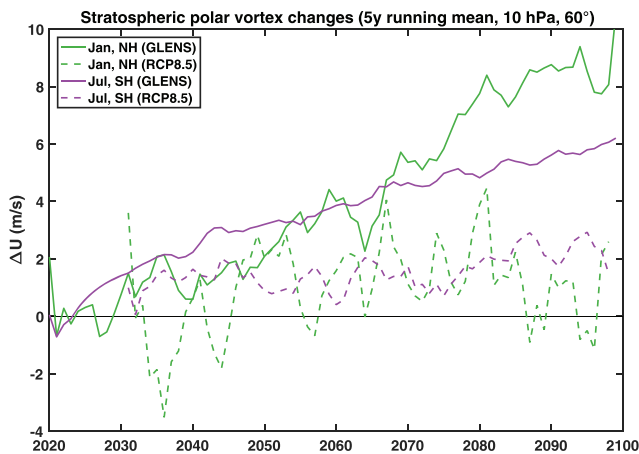
Figure 2. Changes in U winds at 50 hPa at 60° in both hemispheres in the month where the strength of the polar vortex is highest, for both GLENS (straight line) and RCP8.5 (dashed line), compared against the RCP8.5 period between 2010 and 2029.

Figure 1, it is clear that the assumptions of linearity in the response of ℓ_0 and ℓ_1 holds robustly up to approximately 2070, or roughly 30 Tg-SO_2 injected overall, but linearity subsequently breaks down, leading to a decrease in efficiency at high latitudes. For ℓ_2, this happens even earlier (2055) (roughly 20 Tg-SO_2 injected). Because the controller in GLENS was always requesting as large a value of ℓ_2 as possible, this decrease in achievable ℓ_2 directly impacted the ability to maintain T2, the equator-to-pole temperature gradient, leaving some residual increase in temperatures at high latitudes relative to baseline.

Unlike for the equatorial case, this high-latitude effect is not due to microphysical changes in the radius of the sulfate particles, since we show in Figure S2 that the radii change is less at high latitudes compared to tropical latitudes (20% compared to 50% over the course of 60 years of increasing injection rates), compared to the changes in AOD shown in Figure 1. We identify this effect as being due to an overall strengthening of the stratospheric polar vortex due to changes in the thermal wind balance. The stratospheric heating, localized in the tropical stratosphere where most of the sulfate is located (and that presents little seasonal dependence; see Figure S3), heightens the temperature gradient between the tropics and the poles, especially in the polar winter when no solar radiation warms the high latitudes, thereby producing stronger westerly winds, that are a direct consequence of the temperature gradient (Holton, 2004). In Figure 2, we show the strength of the mean zonal wind (U) in the winter months at 50 hPa and 60° latitude both in the NH and SH. Changes in the overall structure of the zonal winds have been noted before (Kravitz et al., 2019; Niemeier et al., 2020; Niemeier & Schmidt, 2017; Richter et al., 2017), but their temporal variations have not been analyzed.

To better identify changes in the transport barrier associated with the polar vortex, we use here Ertel's potential vorticity (PV) as a diagnostic tool. This quantity is defined as

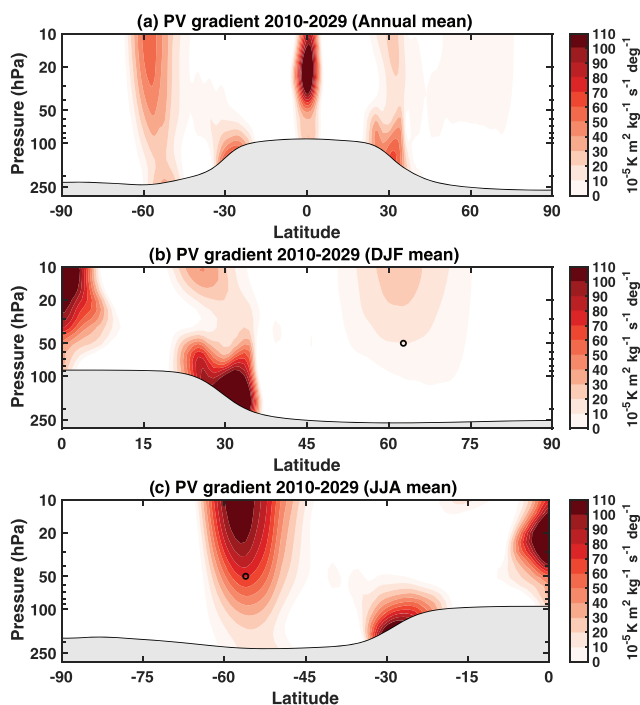$$PV = (\zeta_\theta + f)\left(-g\frac{\partial \theta}{\partial p}\right) \tag{1}$$

and describes the ratio of the absolute vorticity ($\zeta_\theta + f$), where ζ_θ is the vertical component of relative vorticity on an isentropic surface and f is the Coriolis parameter, to $\left(-g\frac{\partial \theta}{\partial p}\right)$, which is a measure of stability, or of the thickness of the isentropic layers (θ is the potential temperature) (Holton, 2004).

It has already been used in the past to further verify changes in the transport of various chemical components in the atmosphere due to circulation changes, especially at high latitudes (Manney et al., 1994; Nash et al., 1996; Ploeger et al., 2015). In the absence of friction and diabatic processes, the PV of an air parcel is materially conserved. Thus, it should be expected that in regions of enhanced PV gradient, there is reduced exchange of air parcels and, therefore, reduced mixing of atmospheric constituents across that gradient (Holton, 2004). Manney et al. (1994) and Nash et al. (1996) proved that this analogy is successful in identifying transport barriers due to strengthening of the stratospheric polar vortex, resulting in reduced mixing of warm air from lower latitudes and, therefore, a cooler polar stratosphere with subsequent ozone destruction. We show in Figure 3 the stratospheric PV gradient in the 2010–2029 period: in it, two transport barriers are present that can be compared with the AOD distribution in Figure 1: one at around 30°N/S, whose effects are clearly visible in the equatorial injection case (Figure 1b) (and whose presence motivated the injection locations in Tilmes, Richter, Kravitz, et al., 2018) and the one we are interested in this work, around 60°N/S in the relative hemispheric winter. The effects of the polar barriers are visible in both injection strategies in Figure 1, and our next analyses will focus on those. An equatorial maximum is also present in Figure 1b, and its interaction with the injected stratospheric aerosols has been discussed in depth in the past (Kravitz et al., 2019; Niemeier et al., 2020; Visioni et al., 2018).

In Figure 4, we show that the PV gradient in both hemispheres in winter has a strong positive anomaly compared to the unperturbed 2010–2029 period that evolves with increasing injection rates. There is a general equatorward shift in this maxima in both hemispheres, with the exception of one decade, 2040–2049, where the Northern Hemisphere (NH) shows a short-lived reversal of this general trend. While the magnitude

Figure 3. PV gradient averaged over the 2010–2029 period in RCP8.5, considering the annual average (panel a) and the average over the NH and SH winter (panels b and c). Areas below the tropopause (black lines, same monthly averages as those indicated in the title) have been shaded in gray. The location of the high-latitudinal maxima of the PV gradient at 50 hPa has been marked with a black circle.

of the maxima in both gradient anomalies increases in both hemispheres in a similar way, the differences in the latitudinal shift could be due to a slight asymmetry in the temperature anomaly in the tropics, due to differences in the injection rates in the hemispheres. In Figures S5 and S6, we further show for each decade the zonal mean PV anomaly at different latitudes and altitudes, highlighting the relationship between PV anomaly and changes in the zonal winds identified in Figure 3. The dynamics and structure of the polar vortex in each hemisphere are different, and also in our case, there could be a variety of reasons why they might not respond exactly the same way. We note that the stratospheric polar vortex is generally already stronger in the Southern Hemisphere (SH) (see Figure S4), and while this is observed also in reanalyses, CESM1(WACCM) has an already identified strong bias in the southern polar vortex (Mills et al., 2017). However, in general, previous validations of this model have demonstrated its capabilities in representing stratospheric dynamics, both for GHG forcings (Dietmuller et al., 2018; Mills et al., 2017) and against previous large tropical volcanic eruptions (Mills et al., 2016, 2017; Tang et al., 2013). Therefore, while the overall magnitude of the change might be overestimated, we feel confident that the the model correctly represents the effect we are observing.

One possible further explanation for both the changes in location and overall inter-hemispheric differences in the evolution over time of the PV anomaly could be found in differences in the ozone response: By 2050, ODS concentrations are projected to reduce following a strong abatement in emissions, resulting in a full recovery of stratospheric ozone (and possible super-recovery, due to stratospheric cooling from GHGs) late in the 21st century (Dhomse et al., 2018). The heating produced by the sulfate aerosols can contribute to ozone destruction (Richter et al., 2017; Tilmes, Richter, Kravitz, et al., 2018) by Cl_y and Br_y, therefore resulting in a net cooling attributable to ozone at high latitudes. When the concentration of ODS is reduced, however, this mechanism of ozone destruction weakens, and ozone is allowed to recover also in the geoengineering case (albeit less than under RCP8.5), resulting in an ozone-induced warming particularly in the SH where ozone destruction is stronger in the 2010–2029 period (Figure S8). The ozone-induced high-latitude positive heating rates after 2050 may partially counter-balance the temperature gradient resulting from the aerosol heating rates at lower latitudes, therefore modifying the changes in the SH stratospheric polar vortex.
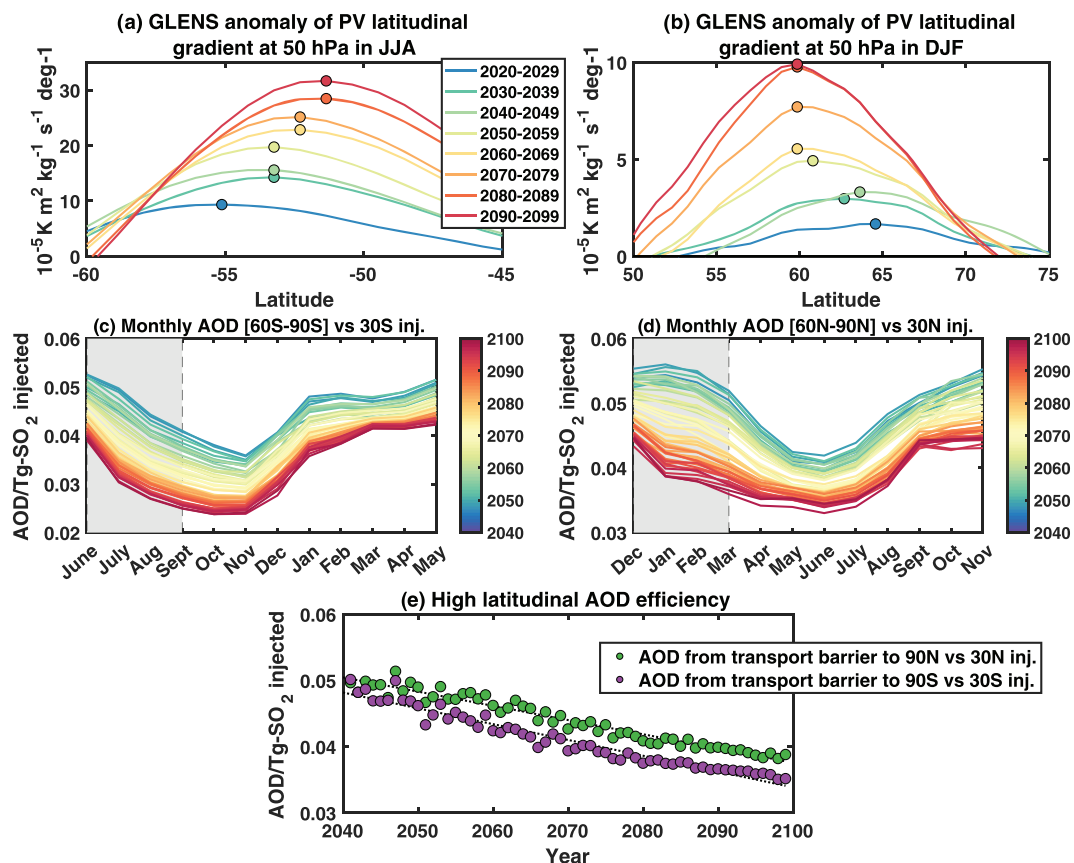
Figure 4. Changes in the PV gradient compared to the 2010–2029 period at 50 hPa in the season where the strength of the polar vortex is higher, (a) DJF, NH and (b) JJA, SH, distinguished by decade (see legend). The average location of the maxima is highlighted in each decade with a circle of the same color. See also Figure S7 for a comparison with the unperturbed PV gradient. (c, d) Monthly AOD from 90° to 60° in both hemispheres, normalized by the injection rate in that year at 30°. Months with the strongest polar vortices, as shown in Figure 3, are shaded in gray. (e) Yearly AOD averaged from 90° to the transport barrier identified using the PV gradient anomalies, normalized by the injection rate in that year at 30°. A graphical linear fit is provided for both quantities.

In Figures 4c and 4d, we highlight the correlation between the polar vortex and the seasonality of high-latitudinal AOD efficiency, defined as the AOD between 90° and 60° divided by the injected SO_2 at 30° (since that drives the AOD at high latitudes, as shown in Figure S6 in Visioni, MacMartin, et al., 2020). This quantity is not constant throughout the year and tends to be at its lowest in summer when wave activity is at its lowest. Its highest values are then reached in autumn and early winter, when mixing is higher, after which a marked decrease in AOD is visible in the winter months. This decrease is heightened by the strengthening of the transport barrier shown in Figures 4a and 4b, thus resulting in lower annual values of AOD, as we show in Figure 4e using the transport barrier identified in the previous discussion to consider the AOD at high latitudes as only that which resides poleward of the latitude of the maximum of the PV anomaly gradient. Normalizing again this AOD to the injection rate at 30° in both hemispheres, a linear decrease can be observed over the considered period resulting in an overall reduction of around 20% in both hemispheres. The PV gradient increase shown in Figures 4a and 4b, however, in the last 10 years of the experiment is 54% compared to the unperturbed period in the SH, and 89% in the NH (see also Figure S7). This suggests that changes in transport might not be the only effect at play and that the overall decrease in AOD efficiency might be tied to other factors, such as the microphysical growth of the aerosols: as shown in Figure S2, for instance, the effective radius increases by 20% in the southern high latitudes and by 30% in the northern high latitudes.

For the last three panels of Figure 4, we only show the values starting in 2040 (as in Figure 1) for two main reasons: One is that before that date, the algorithm that determines the injection rates has not yet converged, resulting in higher year to year differences in the injection rates and in differences in the demand for L1

and L2 (see also Tilmes, Richter, Kravitz, et al., 2018). The second is that, as shown in Figures 4, S5, and S6, changes in the stratospheric vortex are less clear prior to 2040.

4. Conclusions

If sulfate geoengineering is to be investigated as a potential measure to partially counteract the surface warming resulting from the increase in GHGs over this century, particular attention should be devoted to both its potential surface effects (Irvine & Keith, 2020; Simpson et al., 2019) and to understanding its fundamental limitations. A previous work has shown that the effectiveness when injecting sulfate only at the equator is limited for very high injection loads due to microphysical constraints (Niemeier & Timmreck, 2015), modifications of equatorial dynamics (Aquila et al., 2014), and the interplay between these two (Visioni et al., 2018). Injecting at 30° and 15°N/S has been shown to have the potential to reduce some side effects (Kravitz et al., 2019) and to offer further controllability in terms of achievable climate goals through further control of the resulting latitudinal optical depth of the aerosols (Kravitz et al., 2017; MacMartin et al., 2017; Tilmes, Richter, Kravitz, et al., 2018). Even this approach, however, does not completely reduce the warming at high latitudes: This is partially due to an imperfect match between the radiative forcing of the aerosols (dependent on the presence of incoming solar radiation) compared to that of the CO_2 (Govindasamy et al., 2003; Jiang et al., 2019).

Here we show that another factor to consider when discussing potential limitations of SAG is the modification of stratospheric circulation induced by the stratospheric heating, especially that produced by aerosols at high latitudes. We prove that changes to the thermal wind balance result, in our model simulations, in a strengthening of the stratospheric polar vortex, with subsequent increased isolation of polar air resulting in a reduction in the amount of sulfate aerosols that can be moved by the Brewer-Dobson circulation from middle to high latitudes. While this only slightly affects the ability to reduce global mean surface temperatures, it does influence the desired distribution of AOD at high latitude (possibly contributing to the warmer winters at high latitudes discussed in Jiang et al., 2019), resulting in an increased difficulty in maintaining the equator-to-pole temperature gradient that, while mostly corrected by the implemented feedback algorithm, requires a further increase in the injection amount, thus possibly increasing side effects related to sulfate deposition (Visioni, Slessarev, et al., 2020). Furthermore, it also reduces the AOD efficiency: While globally, over 60 years of increasing injection rates, the drop is 15% (and between 30°N/S, it is only 11%) at high latitudes, this drop increases to 22%.

This points to a possible limitation of developing an SAG strategy considering only injections at low altitudes. It might be that, if a certain AOD distribution is desired to avoid excessive warming at high latitudes, a wider array of latitudes is necessary (Dai et al., 2018), and our work shows that, in this case, injecting SO_2 over 60° in both hemispheres might offset the effect of the polar vortex and its eventual amplification produced by the aerosol perturbation.

It is important to recognize that the effect we have analyzed here is most evident for very high injections of SO_2, aimed at offsetting a large warming produced by an extremely high emission scenario. This highlights the fact that sulfate geoengineering should only be safely considered as part of a broader strategy where a more moderate, temporary deployment may avoid surpassing some specific temperature targets and thus should be coupled with a large reduction in emissions (see, for instance, Tilmes et al., 2020) to avoid similar undesired side effects, among others.

Data Availability Statement

All data from the simulations used in this article are available online (https://doi.org/10.5065/D6JH3JXX).

References

Aquila, V., Garfinkel, C. I., Newman, P. A., Oman, L. D., & Waugh, D. W. (2014). Modifications of the quasi-biennial oscillation by a geoengineering perturbation of the stratospheric aerosol layer. *Geophysical Research Letters*, *41*, 1738–1744. https://doi.org/10.1002/2013GL058818

Benduhn, F., Schallock, J., & Lawrence, M. G. (2016). Early growth dynamical implications for the steerability of stratospheric solar radiation management via sulfur aerosol particles. *Geophysical Research Letters*, *43*, 9956–9963. https://doi.org/10.1002/2016GL070701

Budyko, M. I. (1977). *Climatic changes* (p. 244). Washington, DC: American Geophysical Union. https://doi.org/10.1029/SP010

Butchart, N., Cionni, I., Eyring, V., Shepherd, T. G., Waugh, D. W., Akiyoshi, H., et al. (2010). Chemistry-climate model simulations of twenty-first century stratospheric climate and circulation changes. *Journal of Climate*, *23*(20), 5349–5374. https://doi.org/10.1175/2010JCLI3404.1

Crutzen, P. J. (2006). Albedo enhancement by stratospheric sulfur injections: A contribution to resolve a policy dilemma? *Climatic Change*, *77*(3), 211–220. https://doi.org/10.1007/s10584-006-9101-y

Dai, Z., Weisenstein, D. K., & Keith, D. W. (2018). Tailoring meridional and seasonal radiative forcing by sulfate aerosol solar geoengineering. *Geophysical Research Letters*, *45*, 1030–1039. https://doi.org/10.1002/2017GL076472

Dhomse, S. S., Kinnison, D., Chipperfield, M. P., Salawitch, R. J., Cionni, I., Hegglin, M. I., et al. (2018). Estimates of ozone return dates from Chemistry-Climate Model Initiative simulations. *Atmospheric Chemistry and Physics*, *18*(11), 8409–8438.

Dietmuller, S., Eichinger, R., Garny, H., Birner, T., Boenisch, H., Pitari, G., et al. (2018). Quantifying the effect of mixing on the mean age of air in CCMVal-2 and CCMI-1 models. *Atmospheric Chemistry and Physics*, *18*(9), 6699–6720.

Dykema, J. A., Keith, D. W., & Keutsch, F. N. (2016). Improved aerosol radiative properties as a foundation for solar geoengineering risk assessment. *Geophysical Research Letters*, *43*, 7758–7766. https://doi.org/10.1002/2016GL069258

Govindasamy, B., Caldeira, K., & Duffy, P. B. (2003). Geoengineering Earth's radiation balance to mitigate climate change from a quadrupling of CO_2. *Global and Planetary Change*, *37*(1), 157–168. Evaluation, Intercomparison and Application of Global Climate Models http://www.sciencedirect.com/science/article/pii/S0921818102001959

Holton, J. R. (2004). Chapter 4 circulation and vorticity. In J. R. Holton (Ed.), *An introduction to dynamic meteorology*, International Geophysics (Vol. 88, pp. 86–114). London, UK: Academic Press.

Irvine, P. J., & Keith, D. W. (2020). Halving warming with stratospheric aerosol geoengineering moderates policy-relevant climate hazards. *Environmental Research Letters*, *15*(4), 044011.

Jiang, J., Cao, L., MacMartin, D. G., Simpson, I. R., Kravitz, B., Cheng, W., et al. (2019). Stratospheric sulfate aerosol geoengineering could alter the high-latitude seasonal cycle. *Geophysical Research Letters*, *46*, 14,153–14,163. https://doi.org/10.1029/2019GL085758

Keith, D. W., Weisenstein, D. K., Dykema, J. A., & Keutsch, F. N. (2016). Stratospheric solar geoengineering without ozone loss. *Proceedings of the National Academy of Sciences*, *113*(52), 14,910–14,914.

Kleinschmitt, C., Boucher, O., & Platt, U. (2018). Sensitivity of the radiative forcing by stratospheric sulfur geoengineering to the amount and strategy of the SO_2 injection studied with the LMDZ-S3A model. *Atmospheric Chemistry and Physics*, *18*(4), 2769–2786.

Kravitz, B., Lamarque, J.-F., Tribbia, J. J., Tilmes, S., Vitt, F., Richter, J. H., et al. (2017). First simulations of designing stratospheric sulfate aerosol geoengineering to meet multiple simultaneous climate objectives. *Journal of Geophysical Research: Atmospheres*, *122*, 12,616–12,634. https://doi.org/10.1002/2017JD026874

Kravitz, B., & MacMartin, D. G. (2020). Uncertainty and the basis for confidence in solar geoengineering research. *Nature Reviews Earth & Environment*, *1*(1), 64–75. https://doi.org/10.1038/s43017-019-0004-7

Kravitz, B., MacMartin, D. G., Tilmes, S., Richter, J. H., Mills, M. J., Cheng, W., et al. (2019). Comparing surface and stratospheric impacts of geoengineering with different SO_2 injection strategies. *Journal of Geophysical Research: Atmospheres*, *124*, 7900–7918. https://doi.org/10.1029/2019JD030329

Kravitz, B., MacMartin, D. G., Wang, H., & Rasch, P. J. (2016). Geoengineering as a design problem. *Earth System Dynamics*, *7*(2), 469–497.

MacMartin, D. G., Keith, D. W., Kravitz, B., & Caldeira, K. (2013). Management of trade-offs in geoengineering through optimal choice of non-uniform radiative forcing. *Nature Climate Change*, *3*(4), 365–368. https://doi.org/10.1038/nclimate1722

MacMartin, D. G., Kravitz, B., Mills, M. J., Tribbia, J. J., Tilmes, S., Richter, J. H., et al. (2017). The climate response to stratospheric aerosol geoengineering can be tailored using multiple injection locations. *Journal of Geophysical Research: Atmospheres*, *122*, 12,574–12,590. https://doi.org/10.1002/2017JD026868

Manney, G. L., Zurek, R. W., Gelman, M. E., Miller, A. J., & Nagatani, R. (1994). The anomalous arctic lower stratospheric polar vortex of 1992–1993. *Geophysical Research Letters*, *21*(22), 2405–2408. https://doi.org/10.1029/94GL02368

Manzini, E., Karpechko, A. Y., Anstey, J., Baldwin, M. P., Black, R. X., Cagnazzo, C., et al. (2014). Northern winter climate change: Assessment of uncertainty in CMIP5 projections related to stratosphere-troposphere coupling. *Journal of Geophysical Research: Atmospheres*, *119*, 7979–7998. https://doi.org/10.1002/2013JD021403

Mills, M. J., Richter, J. H., Tilmes, S., Kravitz, B., Macmartin, D. G., Glanville, A. A., et al. (2017). Radiative and chemical response to interactive stratospheric sulfate aerosols in fully coupled CESM1(WACCM). *Journal of Geophysical Research: Atmospheres*, *122*, 13,061–13,078. https://doi.org/10.1002/2017JD027006

Mills, M. J., Schmidt, A., Easter, R., Solomon, S., Kinnison, D. E., Ghan, S. J., et al. (2016). Global volcanic aerosol properties derived from emissions, 1990–2014, using CESM1(WACCM). *Journal of Geophysical Research: Atmospheres*, *121*, 2332–2348. https://doi.org/10.1002/2015JD024290

Nash, E. R., Newman, P. A., Rosenfield, J. E., & Schoeberl, M. R. (1996). An objective determination of the polar vortex using Ertel's potential vorticity. *Journal of Geophysical Research*, *101*(D5), 9471–9478. https://doi.org/10.1029/96JD00066

Niemeier, U., Richter, J. H., & Tilmes, S. (2020). Differing responses of the QBO to SO_2 injections in two global models. *Atmospheric Chemistry and Physics Discussions*, *2020*, 1–21. https://doi.org/10.5194/acp-2020-206

Niemeier, U., & Schmidt, H. (2017). Changing transport processes in the stratosphere by radiative heating of sulfate aerosols. *Atmospheric Chemistry and Physics*, *17*(24), 14,871–14,886. https://doi.org/10.1002/2013JD020445

Niemeier, U., Schmidt, H., Alterskjær, K., & Kristjánsson, J. E. (2013). Solar irradiance reduction via climate engineering: Impact of different techniques on the energy balance and the hydrological cycle. *Journal of Geophysical Research: Atmospheres*, *118*, 11,905–11,917. https://doi.org/10.1002/2013JD020445

Niemeier, U., & Timmreck, C. (2015). What is the limit of climate engineering by stratospheric injection of SO_2? *Atmospheric Chemistry and Physics*, *15*(16), 9129–9141. https://doi.org/10.5194/acp-15-9129-2015

Pierce, J. R., Weisenstein, D. K., Heckendorn, P., Peter, T., & Keith, D. W. (2010). Efficient formation of stratospheric aerosol for climate engineering by emission of condensible vapor from aircraft. *Geophysical Research Letters*, *37*, L18805. https://doi.org/10.1029/2010GL043975

Pitari, G., Genova, G. D., Mancini, E., Visioni, D., Gandolfi, I., & Cionni, I. (2016). Stratospheric aerosols from major volcanic eruptions: A composition-climate model study of the aerosol cloud dispersal and e-folding time. *Atmosphere*, *7*, 75. https://doi.org/10.3390/atmos7060075

Ploeger, F., Gottschling, C., Griessbach, S., Grooß, J.-U., Guenther, G., Konopka, P., et al. (2015). A potential vorticity-based determination of the transport barrier in the Asian summer monsoon anticyclone. *Atmospheric Chemistry and Physics*, *15*(22), 13,145–13,159. https://doi.org/10.5194/acp-15-13145-2015

Richter, J. H., Tilmes, S., Mills, M. J., Tribbia, J. J., Kravitz, B., Macmartin, D. G., et al. (2017). Stratospheric dynamical response and ozone feedbacks in the presence of SO$_2$ injections. *Journal of Geophysical Research: Atmospheres*, *122*, 12,557–12,573. https://doi.org/10.1002/2017JD026912

Robock, A. (2000). Volcanic eruptions and climate. *Reviews of Geophysics*, *38*(2), 191–219. https://doi.org/10.1029/1998RG000054

Simpson, I. R., Hitchcock, P., Seager, R., Wu, Y., & Callaghan, P. (2018). The downward influence of uncertainty in the Northern Hemisphere stratospheric polar vortex response to climate change. *Journal of Climate*, *31*(16), 6371–6391. https://doi.org/10.1175/JCLI-D-18-0041.1

Simpson, I. R., Tilmes, S., Richter, J. H., Kravitz, B., MacMartin, D. G., Mills, M. J., et al. (2019). The regional hydroclimate response to stratospheric sulfate geoengineering and the role of stratospheric heating. *Journal of Geophysical Research: Atmospheres*, *124*, 12,587–12,616. https://doi.org/10.1029/2019JD031093

Tang, Q., Hess, P. G., Brown-Steiner, B., & Kinnison, D. E. (2013). Tropospheric ozone decrease due to the Mount Pinatubo eruption: Reduced stratospheric influx. *Geophysical Research Letters*, *40*, 5553–5558. https://doi.org/10.1002/2013GL056563

Tilmes, S., Fasullo, J., Lamarque, J.-F., Marsh, D. R., Mills, M., Alterskær, K., et al. (2013). The hydrological impact of geoengineering in the Geoengineering Model Intercomparison Project (GeoMIP). *Journal of Geophysical Research: Atmospheres*, *118*, 11,036–11,058. https://doi.org/10.1002/jgrd.50868

Tilmes, S., MacMartin, D. G., Lenaerts, J. T. M., van Kampenhout, L., Muntjewerf, L., Xia, L., et al. (2020). Reaching 1.5 and 2.0°C global surface temperature targets using stratospheric aerosol geoengineering. *Earth System Dynamics*, *11*(3), 579–601. https://doi.org/10.5194/esd-11-579-2020

Tilmes, S., Richter, J. H., Kravitz, B., Macmartin, D. G., Mills, M. J., Simpson, I. R., et al. (2018). CESM1(WACCM) stratospheric aerosol geoengineering large ensemble project. *Bulletin of the American Meteorological Society*, *99*(11), 2361–2371.

Tilmes, S., Richter, J. H., Mills, M. J., Kravitz, B., MacMartin, D. G., Garcia, R. R., et al. (2018). Effects of different stratospheric SO$_2$ injection altitudes on stratospheric chemistry and dynamics. *Journal of Geophysical Research: Atmospheres*, *123*, 4654–4673. https://doi.org/10.1002/2017JD028146

Tilmes, S., Richter, J. H., Mills, M. J., Kravitz, B., Macmartin, D. G., Vitt, F., et al. (2017). Sensitivity of aerosol distribution and climate response to stratospheric SO$_2$ injection locations. *Journal of Geophysical Research: Atmospheres*, *122*, 12,591–12,615. https://doi.org/10.1002/2017JD026888

Vattioni, S., Weisenstein, D., Keith, D., Feinberg, A., Peter, T., & Stenke, A. (2019). Exploring accumulation-mode H$_2$SO$_4$ versus SO$_2$ stratospheric sulfate geoengineering in a sectional aerosol-chemistry-climate model. *Atmospheric Chemistry and Physics*, *19*(7), 4877–4897. https://doi.org/10.5194/acp-19-4877-2019

Visioni, D., MacMartin, D. G., Kravitz, B., Richter, J. H., Tilmes, S., & Mills, M. J. (2020). Seasonally modulated stratospheric aerosol geoengineering alters the climate outcomes. *Geophysical Research Letters*, *47*, e2020GL088337. https://doi.org/10.1029/2020GL088337

Visioni, D., Pitari, G., Aquila, V., Tilmes, S., Cionni, I., Di Genova, G., & Mancini, E. (2017). Sulfate geoengineering impact on methane transport and lifetime: Results from the Geoengineering Model Intercomparison Project (GeoMIP). *Atmospheric Chemistry and Physics*, *17*(18), 11,209–11,226. https://doi.org/10.5194/acp-17-11209-2017

Visioni, D., Pitari, G., Tuccella, P., & Curci, G. (2018). Sulfur deposition changes under sulfate geoengineering conditions: Quasi-biennial oscillation effects on the transport and lifetime of stratospheric aerosols. *Atmospheric Chemistry and Physics*, *18*, 2787–2808. https://doi.org/10.5194/acp-18-2787-2018

Visioni, D., Slessarev, E., MacMartin, D., Mahowald, N. M., Goodale, C. L., & Xia, L. (2020). What goes up must come down: Impacts of deposition in a sulfate geoengineering scenario. *Environmental Research Letters*. https://doi.org/10.1088/1748-9326/ab94eb

Waugh, D. W., Sobel, A. H., & Polvani, L. M. (2017). What is the polar vortex and how does it influence weather? *Bulletin of the American Meteorological Society*, *98*(1), 37–44.

Wu, Y., Simpson, I. R., & Seager, R. (2019). Intermodel spread in the Northern Hemisphere stratospheric polar vortex response to climate change in the CMIP5 models. *Geophysical Research Letters*, *46*, 13,290–13,298. https://doi.org/10.1029/2019GL085545